stall control system to delay wing stall in an unsteady environment. Pressure sensors S1 and S5, location shown in Table 1, were used by the controller in the closed-loop flow control demonstration. During the α sweep of the wing at 2 deg/s, it was observed that with increasing α, flow separation successively progressed from the trailing edge toward the leading edge of the wing, as shown in a series of snapshots in Fig. 10. Figure 10 shows that, as α was increased from 13 to 23 deg, the pressure sensors, which are represented by light emitting diodes, lit up at the trailing edge before those at the leading edge, confirming the STDEV-based control law for detection of critical flow conditions. As can be inferred from Fig. 10, leading-edge separation occurred at $\alpha = 18$ deg. The controller triggered the actuation of DFEs at $\alpha = 18$ deg, forcing flow reattachment and a delay in stall angle up to $\alpha = 20$ deg. For $\alpha \geq 21$ deg, the wing was completely stalled, and the DFEs had no effect on the fluid flow.

The results presented in this Note are for a low Reynolds number incompressible flow case where the influence of three-dimensional flow caused due to wing sweep and wing taper on the reliability of STDEV technique are not fully examined. Nevertheless, it is shown that the frequency characteristics of imminent flow separation is a function of sensor location on the wing surface, and these characteristics transpire into flow-separation signature in the form of STDEV thresholds, which are distinct for each sensor location. As this approach evolves further, advanced signal processing techniques such as a recursively fit autoregressive moving average exogenous system identification model or the short-time Fourier transform model will be used to create more sophisticated stall signature definitions for three-dimensional crossflow conditions. As for dynamic maneuvers, modular arrays of colocated sensors, actuators, and local controllers will need to be coordinated to maintain a desired flow effect.

Conclusions

Proof-of-concept experiments for an active transparent stall control system were successfully conducted on a 30-deg sweep NACA 0020 wing in a low-speed wind tunnel. The control system consisted of fast-response pressure sensors, deployable flow control devices, and a closed-loop controller. Findings on the distinctive nature of pressure fluctuations during prestall conditions served as the actuating signal for the controller to trigger the leading-edge flow control devices. Results from open-loop experiments demonstrated significant increase in the upper surface suction levels before wing stall, causing a delay in the stall angle. Closed-loop experiments demonstrated the ability of the controller to detect actively the onset of wing stall and employed flow effectors to control separation and delay stall, in real time. Successful application of such transparent stall control systems on control surfaces will lead to improved aerodynamic performance of both conventional and unconventional air vehicles.

Acknowledgments

The authors thank Frederick Lisy, Troy Prince, Jack DiCocco, and Reed Carver of Orbital Research, Inc., for supporting portions of this research under Grant F33615-99-C-3008 from the U.S. Air Force Research Laboratory at Wright–Patterson Air Force Base.

References

[1]Gad-el-Hak, M., *Flow Control: Passive, Active, and Reactive Flow Management*, 1st ed., Cambridge Univ. Press, Cambridge, England, U.K., 2000, pp. 150–188.

[2]McMichael, J. M., "Progress and Prospects of Active Flow Control Using Microfabricated Electromechanical Systems," AIAA Paper 96-0306, Jan. 1996.

[3]Lin, J. C., Robinson, S. K., McGhee, R. J., and Valarezo, W. O., "Separation Control on High-Lift Airfoils Via Micro-Vortex Generators," *Journal of Aircraft*, Vol. 31, No. 6, 1994, pp. 1317–1323.

[4]Schmidt, R., and Fellenstein, J., "Microactuator Arrays for Adaptable Control Surfaces," Final Rept., Advanced Research Projects Agency, Ord. No. 5916, U.S. Army Missile Command, Contract DAAH01-92-C-R207, 1992.

[5]Lisy, F. J., Carver, R., and Prince, T. S., "Smart Surfaces For Flow Control Arrays," Final Rept., Phase I U.S. Air Force Small Business Innovation Research Contract F33615-98-C-3006, Jan. 1999.

[6]Patel, M. P., Carver, R., Lisy, F. J., Prince, T. S., and Ng, T. T., "Detection and Control of Flow Separation Using Pressure Sensors and Micro-Vortex Generators," AIAA Paper 2002-0268, Jan. 2002.

[7]Patel, M. P., Prince, T. S., Ng, T. T., and Lisy, F. J., "Control of Aircraft Stall via Embedded Pressure Sensors and Deployable Flow Effectors," AIAA Paper 2002-3170, June 2002.

Navier–Stokes-Based Study into Linearity in Transonic Flow for Flutter Analysis

Roberto G. A. Silva,* Olympio A. F. Mello,† and João L. F. Azevedo‡
Centro Técnico Aeroespacial, 12228-904 São José dos Campos SP, Brazil

Introduction

IT has been known for quite some time[1] that transonic flow conditions are critical for flutter, with the flutter dynamic pressure being substantially reduced for Mach numbers near unity, in a phenomenon usually termed as "transonic dip."[2] The severity of flutter at transonic speeds is linked to the presence of moving shock waves over the wing surface.[3] From these considerations it is clear that accurate flutter predictions depend on the ability of predicting correct shock strength and location in a time-accurate fashion. In recent years there has been increased emphasis on the use of computational-fluid-dynamics procedures to accomplish such task.

Most flutter computations use commercial finite element codes with aeroelastic modeling capability such as NASTRAN™. These codes, however, are usually based on linear aerodynamic methods and thus limited to subsonic or supersonic analysis. Transonic flutter clearance relies on experience combined with costly and time-consuming wind tunnel and/or flight tests. More recently, computational aeroelasticity has allowed coupled aerodynamic/structural dynamic computations in the transonic regime. However, the computational resources needed for this coupled analysis are quite significant, and so its industrial application is still limited.[4]

Efforts to provide viable alternatives to these costly analyses and tests have been reported in the literature. These methods approximately model transonic nonlinear aerodynamics and are based on corrections of the linear aerodynamic influence coefficient matrix. The Transonic Equivalent Strip method (TES)[5] is one approach that shows good results in predicting the transonic dip phenomenon. The TES method is based on the application of two consecutive correction steps: chordwise (mean flow) and spanwise (phase correction) to a given steady mean pressure input from measured or computed data. Another approach is the local equivalence concept,[6] which is based in an optimization procedure using computed or wind-tunnel results.

Pitt and Goodman[7] developed modifications of doublet-lattice influence coefficients using results from a transonic-small-disturbance code. That method was capable of simulating the transonic dip phenomenon with small differences with respect to wind-tunnel data.

Received 25 November 2002; revision received 13 May 2003; accepted for publication 14 May 2003.

*Research Engineer, Aeronautical Systems Division, Instituto de Aeronáutica e Espaço; rasilva@iae.cta.br.

†Senior Research Engineer, Instituto de Aeronáutica e Espaço; oamello@iae.cta.br.

‡Senior Research Engineer, Head of Aerodynamics Sub-Division, Space Systems Division, Instituto de Aeronáutica e Espaço. Senior Member AIAA.

These discrepancies were attributed by the authors to viscous effects. Indeed, viscous effects alter the strength and location of shock waves over the wing surface, which in turn can have a significant effect on the flutter computations. To take viscous effects into account, Silva et al.[8] used results from viscous simulations to modify the doublet-lattice influence coefficients.

Approximate flutter analyses in transonic flow typically employ a linear flutter package with the inclusion of the nonlinear transonic effects, by applying corrections to the aerodynamic influence coefficient matrices. However, such analyses implicitly require that transonic aerodynamic loads are "locally" linear with respect to structural deformation about a given geometry. This linear behavior has been shown[9] in two-dimensional flow for small dynamic angles of attack with a transonic small-disturbance code. The results from that work allowed a "linear boundary" to be established and appeared to justify using the approximate flutter analyses.

In the present work a numerical Navier–Stokes code is used in order to verify the locally linear behavior of aerodynamic loads with respect to the dynamic angle of attack. With the present numerical technique viscous and three-dimensional effects are taken into account and shown to be significant.

Numerical Method

The Navier–Stokes solver used in the present work is a modified version of a code developed by Sankar and Kwon.[10] Such modified methodology has been published elsewhere[11] and is not described here.

The numerical method has been previously validated against experimental data[12] for the case of a model of the F-5 wing at several Mach numbers up to 0.95 oscillating at frequencies of 20 and 40 Hz. Good agreement in unsteady pressure coefficients was observed over all wing stations, although a few discrepancies were noted for stations near the wing tip, as a result of difficulties in obtaining a smooth grid around the wing tip within reasonably economical grid sizes. For consistency, the same boundary conditions were employed in the present work, namely, no slip at the solid surface, approximate nonreflective conditions at the far field, and no-slip wall boundary conditions at the wing root because the validation was for a wind-tunnel model.

Test Cases and Data Treatment

The numerical procedure has been applied to the F-5 wing oscillating in rigid pitch around an axis perpendicular to the root midchord. Pitch amplitudes, also denoted here as dynamic angles of attack, were 0.125 to 1.5 deg, in equal steps of 0.125 deg. Oscillations were simulated around a steady-state angle $\alpha_0 = 0.0$ deg. For all test cases presented here the Mach number was 0.95, and the Reynolds number $Re = \rho_\infty U_\infty c_r / \mu_\infty$ was 11×10^6, scaled by the root chord $c_r = 0.6396$ ms.

The reduced frequency k is defined as the ratio of the circular frequency ω times a reference chord c by the speed of the sound a_∞. In this work simulations were conducted for reduced frequencies of 0.10, 0.15 0.20, 0.25, and 0.30. After the unsteady pressures are acquired, a discrete Fourier transformation is used to obtain the frequency-domain components (real and imaginary parts). Similar transformations are applied to the lift coefficient C_L and moment coefficient C_M about the quarter-chord.

The shock position along the wing section chord is determined by using the criterion of maximum pressure coefficient gradient over the chord. The grid resolution in the region around the shock is coarse; thus, a polynomial interpolation is needed in order to find the maximum gradient position. A polynomial interpolation of third degree was chosen in order to yield a linear expression for the second derivative with respect to the nondimenstional chordwise coordinate, from which the maximum gradient position can be found. The points employed in the interpolation are chosen to be nearby the shock location, taking into account its displacement.

After the shock location history with time is determined, Fourier transformations are applied to shock displacement in the time domain.

During the present investigation, it was found that obtaining frequency content for the aerodynamic coefficients C_p, C_L, and C_M gave more consistent results than the ones for the shock position, which depends on how good the polynomial interpolation is. Inadequate polynomials would easily result in spurious shock positions.

Results

Three representative spanwise stations at 35.5, 72.1, and 97.7% were chosen for the present investigation. Figure 1 presents a sample time history for the pressure coefficient differential at the three chosen spanwise stations for a dynamic angle of attack $\Delta\alpha = 1.0$ deg and reduced frequency $k = 0.10$. It can be observed that the pressure coefficient time response is not in a single harmonic of the movement frequency, especially near the wing tip. This indicates a nonlinear, hysteresis-like behavior. Also, three-dimensional effects are clearly present, as a one-harmonic sinusoidal behavior is evident at the inboard station.

The frequency contents corresponding to that pressure coefficient time history are presented in Figs. 2 (amplitudes) and 3 (phase angles) for the three spanwise stations under consideration. Even though the first harmonic is dominant for all stations, the ones near

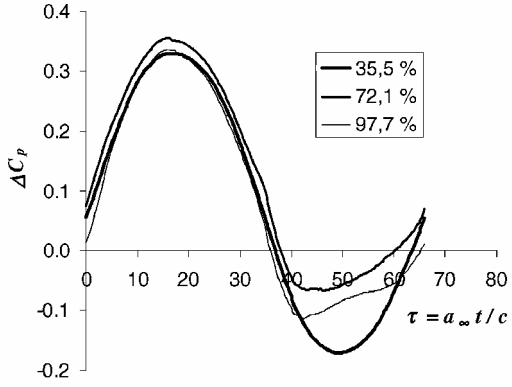

Fig. 1 Differential pressure coefficient time history over F-5 wing ($M = 0.95$, $\Delta\alpha = 1.0$ deg, $k = 0.1$).

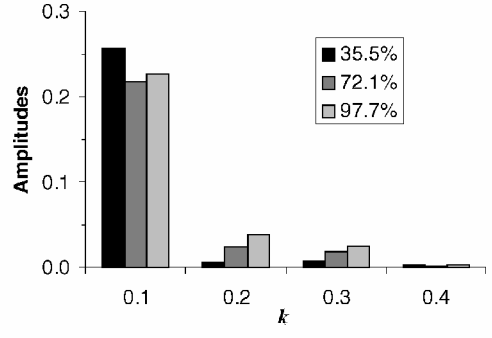

Fig. 2 Frequency contents (amplitudes) of differential pressure coefficient over F-5 wing ($M = 0.95$, $\Delta\alpha = 1.0$ deg, $k = 0.1$).

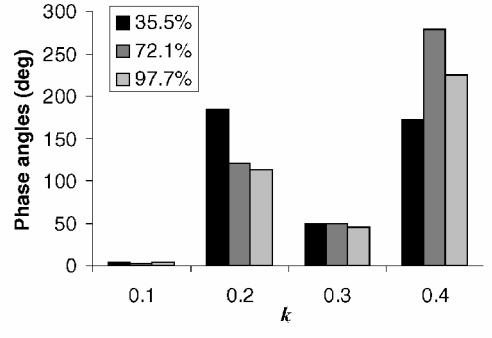

Fig. 3 Frequency contents (phase angles) of differential pressure coefficient over F-5 wing ($M = 0.95$, $\Delta\alpha = 1.0$ deg, $k = 0.1$).

the tip have significant components in the second and third harmonics. Also, these higher harmonics are out of phase with respect to the wing motion.

These higher harmonic effects are not included in linear methods such as the doublet-lattice method, and correction methods based on modification of the aerodynamic influence coefficient matrices[13] would not be readily adaptable to incorporate higher-harmonic corrections. However, there are situations where a second mode is close to a multiple of a first mode. In such case the presence of a second harmonic in the lower-mode aerodynamic response can facilitate the exchange of energy between the modes and be a contributing factor to coalescence.

As mentioned in the preceding section, several test cases were simulated. The aim was to establish the limit for linear behavior with dynamic angle of attack for the range of reduced frequencies tested and at each spanwise station, so that three-dimensional effects could be identified.

For example, at reduced frequency 0.2 the first harmonic of the response in lift and moment coefficients, upper- and lower-surface shock motion were computed for the various dynamic angles of attack.

The results for station 35.5% span are shown in Figs. 4 and 5 for the amplitudes and phase angles, respectively, of aerodynamic coefficients and shock motion. Linear trend lines are placed in the amplitude plot to illustrate deviations from linear behavior. Those are not drawn in the phase plot because during the analysis of the phase-lag variation a basic linear behavior could not be established, and thus a deviation from linearity could not be characterized.

To identify the limit for each case, a linear equation was estimated so that it would start at the origin and pass through the first and second points, which corresponded to a dynamic angles of attack of 0.125 and 0.250 deg. A linear equation was then reduced for these first values, at which the linear behavior would be expected. Then these linear relationship is used to extrapolate to the following points, and a percent deviation of the actual unsteady coefficient or shock displacement to the extrapolated value was computed. The first point in which the deviation exceeded 5% and the point before

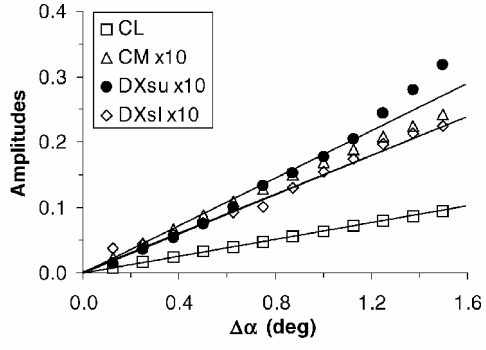

Fig. 4 Effect of dynamic angle of attack on unsteady aerodynamic coefficients and shock motion (amplitudes; station 35.5%; $k = 0.2$).

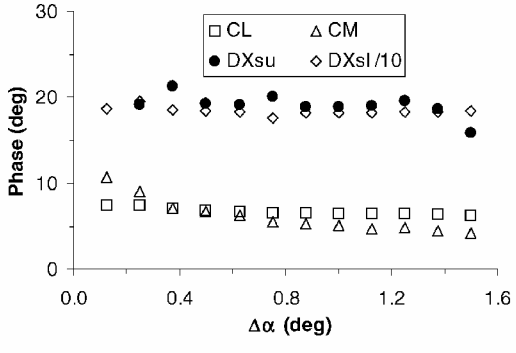

Fig. 5 Effect of dynamic angle of attack on unsteady aerodynamic coefficients and shock motion (phase angles; station 35.5%; $k = 0.2$).

that were used in an interpolation to find the dynamic angle of attack where the linear limit was.

Two criteria were used to establish the linear boundary: 5% deviation in pitching-moment amplitude and 5% deviation in shock motion amplitude. The latter criterion is used only for the upper surface. The lower-surface shock is weaker than the upper-surface one because the wing profile is asymmetric. The shock movement then presents a significant dispersion probably promoted by the turbulent boundary layer.

Using the preceding criteria, the linear limits for the test cases corresponding to Figs. 4 and 5, that is, reduced frequency 0.2 and station 35.5%, were found to be $\Delta\alpha = 0.61$ deg for the pitching-moment criterion and $\Delta\alpha = 0.58$ deg for the shock-displacement criterion.

Plots similar to Figs. 4 and 5 were prepared for stations 72.1 and 97.7%. These plots are not shown here because of space constraints. At 72.1% it was observed that deviation from linear behavior has occurred at smaller dynamic angles. Indeed, using the procedure just described yielded linear limits of $\Delta\alpha = 0.34$ deg for the pitching-moment criterion and $\Delta\alpha = 0.50$ deg for the shock-displacement criterion.

At station 97.7% the deviation from linear behavior seems to occur even earlier than before in terms of dynamic angles. For this case the computed linear limits are $\Delta\alpha = 0.32$ deg for the pitching-moment criterion and $\Delta\alpha = 0.27$ deg for the shock-displacement criterion. Even though the results at the outboard station should be regarded with caution, the results just described show that the linear boundary is more restrictive for outboard stations. Three-dimensional effects are therefore significant, and using two-dimensional linear boundaries in a general problem would seem to be questionable. Shock strength increases with the proximity to the wing tip. Then, the linear boundary could be affected by the upper-surface shock strength.

Simulations for the several reduced frequencies with the corresponding determination of linear limits allow for a comparison of these limits at different spanwise stations using both linearity criteria. This is illustrated in Fig. 6, where the linear boundaries are plotted against reduced frequency for the three spanwise stations (35.5, 72.1, and 97.7%) for the pitching moment and Fig. 7 for the upper-surface shock displacement criteria.

The results shown in Figs. 6 and 7 indicate that the shock-displacement criterion is more conservative than the pitching-moment criterion, as found by Dowell et al.[9] In addition, the linear boundaries based on both pitching-moment and shock-displacement criteria clearly depend on the spanwise station. For the first criterion, at the inner station the behavior is similar to the two–dimensional, inviscid case as presented by Dowell et al.[9] For outer spanwise stations the shock is stronger, and three-dimensional effects are more pronounced. Consequently, the linear behavior is affected, as can be noted in Fig. 6. A somewhat surprising result is that the shock movement-based linear limit does not seem to increase with reduced frequency for the inner stations and even decreases with reduced frequency for the outer station.

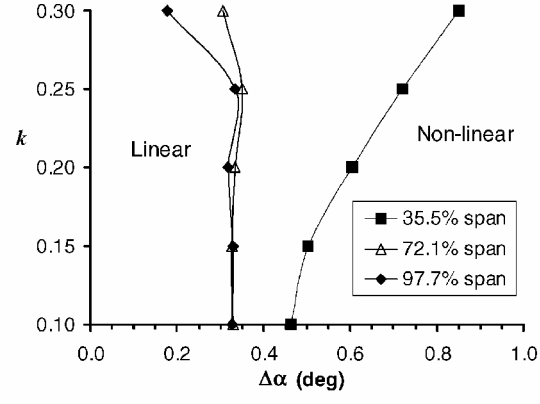

Fig. 6 Boundaries for linear behavior based on the C_M criteria.

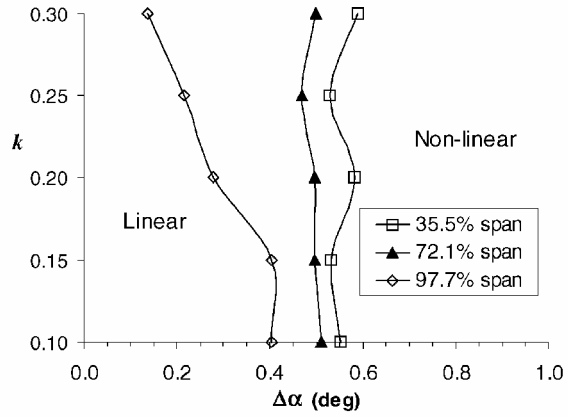

Fig. 7 Boundaries for linear behavior based on the shock-displacement criteria.

Conclusions

Simulations of unsteady transonic flow over the F-5 wing model were performed in order to study the linearity of unsteady loads and shock displacement with dynamic angle-of-attack amplitude and frequency. The aerodynamic response and shock displacement were found to include higher harmonics, which are usually not considered in correction procedures applied to linear aeroelastic methods.

In flutter analysis there are situations in which a second mode is close to a multiple of a first mode. In such case the presence of a second harmonic in the lower-mode aerodynamic response can facilitate the exchange of energy between the modes and be a contributing factor to coalescence. For this reason the present results seem to indicate the need for considering such harmonics in future correction methods.

Linear boundaries were computed for a few reduced frequencies and spanwise stations along the wing, using two criteria, based on moment coefficient and shock displacement. These boundaries were found to be more conservative for the shock-displacement criterion. The linear limits calculated using the moment coefficient criterion were found to depend significantly on the spanwise station. This indicates that simply using two-dimensional linear limits would not be appropriate when dealing with correction methods.

Notwithstanding the dependence of the linear limits on reduced frequency and spanwise station, it is clear that some degree of linear behavior can be assumed for aeroelastic methods that employ corrected coefficients. However, this assumption of linearity should be used with caution and would not apply to problems such as aeroelastic response or limit cycle, unless the amplitude of deformation is kept below previously identified linear limits that take into account reduced frequency and spanwise station.

Acknowledgments

The authors would like to thank Luciano Amaury dos Santos for his help in processing the data. The second and third authors were supported by the Conselho Nacional de Desenvolvimento Científico e Tecnológico (CNPq), Brazil, under the Integrated Project Research Grant No. 522.413/96-0.

References

[1]Landahl, M. T., *Unsteady Transonic Flow*, Pergamon, New York, 1951.

[2]Whitlow, W., Jr., "Computational Unsteady Aerodynamics for Aeroelastic Analysis," NASA TM-100523, Dec. 1987.

[3]Ashley, H., "Role of Shocks in the 'Sub-Transonic' Flutter Phenomenon," *Journal of Aircraft*, Vol. 17, No. 3, 1980, p. 187.

[4]Sankar, L. N., Bharadvaj, B. K., and Tsung, F.-L., "A Three Dimensional Navier–Stokes/Full-Potential Coupled Analysis for Viscous Transonic Flows," *AIAA Journal*, Vol. 31, No. 10, 1993.

[5]Liu, D. D., Kao, Y. F., and Fung, K. Y., "An Efficient Method for Computing Unsteady Transonic Aerodynamics of Swept Wings with Control Surfaces," *Journal of Aircraft*, Vol. 25, No. 1, 1988, pp. 25–31.

[6]Baker, M. L., Yuan, K., and Goggin, P. J., "Calculation of Corrections to Linear Aerodynamic Methods for Static and Dynamic Analysis and Design," AIAA Paper 98-2072, 1998.

[7]Pitt, D. M., and Goodman, C. E., "Flutter Calculations Using Doublet Lattice Aerodynamics Modified by the Full Potential Equations," AIAA Paper-87-0882-CP, 1987.

[8]Silva, R. G. A., Mello, O. A. F., and Azevedo, J. L. F., "Transonic Flutter Calculations Based on Assumed Mode Shapes Corrections," *Proceedings of the CEAS/AIAA International Forum on Aeroelasticity and Structural Dynamics*, AIAA, Reston, VA, 2001, pp. 183–194.

[9]Dowell, E. H. (ed.), Crawley, E. F., Curtiss, H. C., Jr., Peters, D. A., Scanlan, R. H., and Sisto, F., *A Modern Course in Aeroelasticity*, 3rd ed., Kluwer, Dordrecht, The Netherlands, 1995, pp. 472–487.

[10]Sankar, L. N., and Kwon, O. J., "High-Alpha Simulation of Fighter Aircraft," *Proceedings of the NASA High Angle-of-Attack Technology Conference*, Vol. 1, Pt. 2, NASA Langley Research Center, Hampton, VA, 1990, pp. 689–702.

[11]Mello, O. A. F., and Sankar, L. N., "Computation of Unsteady Transonic Flow over a Fighter Wing Using a Zonal Navier–Stokes/Full-Potential Method," *International Journal for Numerical Methods in Fluids*, Vol. 29, No. 5, 1999, pp. 575–585.

[12]Tijdeman, H., van Nunen, J. W. G., Kraan, A. N., Persoon, A. J., Poestkoke, R., Roos, R., Schippers, P., and Siebert, C. M., "Transonic Wind Tunnel Tests on an Oscillating Wing with External Stores, Part II: Clean Wing," Air Force Flight Dynamics Lab., AFFDL-TR-78-194, Part II, Wright–Patterson AFB, OH, 1979; also NLR-TR-78106-U, Part II.

[13]Palacios, R., Climent, H., Karlsson, A., and Winzell, B., "Assessment of Strategies for Correcting Linear Unsteady Aerodynamics Using CFD or Test Results," *Proceedings of the CEAS/AIAA International Forum on Aeroelasticity and Structural Dynamics*, AIAA, Reston, VA, 2001, pp. 195–210.

Advantages of a Bristled Wing as a Rotary Wing

S. Sunada*
Osaka Prefecture University, Osaka 599-8531, Japan
K. Kawachi†
University of Tokyo, Tokyo 113-8656, Japan
and
K. Yasuda‡
Nihon University, Chiba 274-8501, Japan

Introduction

RECENTLY, the Defense Advanced Research Projects Agency in the United States proposed developing a centimeter-sized insect-like flying machine.[1–3] In the future millimeter-sized flying machines will be indispensable for obtaining information in environments not readily accessible to people, such as hazardous or confined areas. Sunada et al.[4] recently studied the flight of the thrips, which is a millimeter-sized insect. They investigated the fluid-dynamic characteristics of a model bristled wing whose planform is proportional to that of a real thrips' fore wing and where cylinders are used to simulate actual bristles. The characteristics were then compared with those of a solid wing whose planform included the addition of membranes between the cylinders of the wing. Their results reveal that the fluid-dynamic forces acting on the bristled wing are smaller than those on the solid wing during constant-velocity translation,

Received 5 December 2002; revision received 30 May 2003; accepted for publication 5 June 2003.

*Associate Professor, Department of Aerospace Engineering, Graduate School of Engineering; sunada@aero.osakafu-u.ac.jp.

†Professor, Department of Aeronautics and Astronautics. Associate Fellow AIAA.

‡Associate Professor, Department of Aerospace Engineering, College of Science and Technology. Senior Member AIAA.